THE JOURNAL OF PHYSICAL CHEMISTRY A
A JOURNAL OF THE AMERICAN CHEMICAL SOCIETY

pubs.acs.org/JPCA
Article

Kinetics of the Gas-Phase Reactions of *syn*- and *anti*-CH_3CHOO Criegee Intermediate Conformers with SO_2 as a Function of Temperature and Pressure

Rachel E. Lade, Lavinia Onel, Mark A. Blitz, Paul W. Seakins, and Daniel Stone*

Cite This: *J. Phys. Chem. A* 2024, 128, 2815−2824
Read Online

ACCESS | Metrics & More | Article Recommendations | Supporting Information

ABSTRACT: Kinetics of reactions between SO_2 and CH_3CHOO Criegee intermediate conformers have been measured at temperatures between 242 and 353 K and pressures between 10 and 600 Torr using laser flash photolysis of $CH_3CHI_2/O_2/N_2/SO_2$ gas mixtures coupled with time-resolved broadband UV absorption spectroscopy. The kinetics of *syn*-CH_3CHOO + SO_2 are pressure-dependent and exhibit a negative temperature dependence, with the observed pressure dependence reconciling apparent discrepancies between previous measurements performed at ∼298 K. Results indicate a rate coefficient of $(4.80 \pm 0.46) \times 10^{-11}$ cm^3 s^{-1} for the reaction of *syn*-CH_3CHOO with SO_2 at 298 K and 760 Torr. In contrast to the behavior of the *syn*-conformer, the kinetics of *anti*-CH_3CHOO + SO_2 display no significant dependence on temperature or pressure over the ranges investigated, with a mean rate coefficient of $(1.18 \pm 0.21) \times 10^{-10}$ cm^3 s^{-1} over all conditions studied in this work. Results indicate that the reaction of *syn*-CH_3CHOO with SO_2 competes with unimolecular decomposition and reaction with water vapor in areas with high SO_2 concentration and low humidity, particularly at lower temperatures.

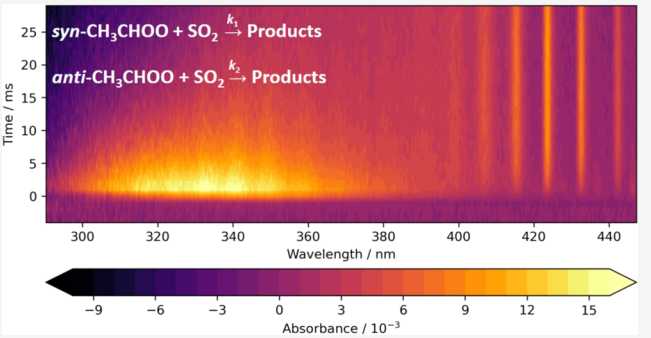

INTRODUCTION

The chemistry of Criegee intermediates (R_2COO) exerts potential impacts on air quality and climate through their involvement in atmospheric oxidation processes, and there has been considerable interest in the potential production of sulfate aerosols resulting from the reactions of Criegee intermediates with sulfur dioxide (SO_2) in the gas phase. Production of Criegee intermediates in the atmosphere occurs following the oxidation of unsaturated volatile organic compounds (VOCs) by ozone (O_3), with the Criegee intermediate initially produced with high internal energy.[1] Collisional stabilization of the nascent Criegee intermediate occurs in competition with unimolecular decomposition, leading to the production of stabilized Criegee intermediates (SCIs), which can participate in a range of processes, including reactions with SO_2.[1,2]

For the reaction of the simplest SCI, CH_2OO, with SO_2, there is now general consensus regarding the kinetics at room temperature, with a current IUPAC recommendation of $(3.7^{+0.45}_{-0.40}) \times 10^{-11}$ cm^3 s^{-1} at 298 K.[3] The kinetics of CH_2OO + SO_2 have been demonstrated to be independent of pressure under typical atmospheric conditions,[4,5] with a negative temperature dependence[6] and reaction products dominated by formaldehyde (HCHO)[4,7] and sulfur trioxide (SO_3).[8,9] Theory indicates that the reaction of an SCI with SO_2 proceeds via the barrierless formation of a cyclic secondary ozonide (SOZ), followed by collisional stabilization of the SOZ or further rearrangement via one or more submerged barriers to form products including SO_3.[10−15] In the case of CH_2OO + SO_2, there is negligible stabilization of the SOZ under atmospheric conditions,[11,12] and contributions from two stereochemical pathways lead to the production of HCHO + SO_3 via submerged barriers.[12] For reactions of other SCIs with SO_2, there is greater potential for stabilization of the SOZ,[11] leading to the potential for pressure-dependent kinetics and product yields.[11]

The atmospheric oxidation of SO_2 by CH_2OO is now expected to be limited, owing to competition with the rapid reaction of CH_2OO with water dimers,[3] but several field studies have demonstrated that significant discrepancies between measured and modeled concentrations of gas-phase sulfuric acid (H_2SO_4) in the atmosphere remain, which potentially result from incomplete consideration of the

Received: January 10, 2024
Revised: February 19, 2024
Accepted: March 13, 2024
Published: March 29, 2024

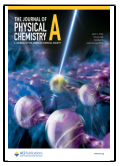

https://doi.org/10.1021/acs.jpca.4c00199
J. Phys. Chem. A 2024, 128, 2815−2824

Table 1. Summary of Literature Results for k_1 and k_2[a]

reference	method	photolysis λ/nm	T/K	p/Torr	bath gas	$[CH_3CHI_2]/10^{13}$ cm^{-3}	$[SO_2]/10^{13}$ cm^{-3}	$k_1/10^{-11}$ cm^3 s^{-1}	$k_2/10^{-10}$ cm^3 s^{-1}
Taatjes et al.[25]	LFP/PIMS	351	298	4	He		0.7−5	2.4 ± 0.3	0.67 ± 0.10
Smith et al.[28]	LFP/UV abs	248	295	7.5−500	N_2	1300	155−600	2.0 ± 0.3	
Sheps et al.[26]	LFP/UV abs	266	293	10	He	1.5	0.8−4.8	2.9 ± 0.3	2.2 ± 0.2
Howes et al.[5]	LFP/PIMS	248	295	1−2.5	N_2	1−10	2−9	1.7 ± 0.3	
Zhou et al.[27]	LFP/LIF	248	298	10	Ar	1.9−10.4	0.3−2.2	2.5 ± 0.2	

[a]LFP = laser flash photolysis, PIMS = photoionization mass spectrometry, UV abs = ultraviolet absorption.

chemistry of SCIs other than CH_2OO.[16−19] Measurements in a boreal forest in Finland led to the suggestion that reactions of SCIs with SO_2 may have been responsible for up to 50% of the H_2SO_4 observed in the gas phase,[16,17] while observations in a rural location in Germany have indicated that SCI + SO_2 reactions could be responsible for up to 80% of H_2SO_4 produced at night.[17] Similarly, field experiments in Texas, United States, have suggested that nighttime production of H_2SO_4 is dominated by SCI + SO_2 reactions, with potentially important contributions in the afternoon,[18] and agreement between observations and model predictions for sulfate aerosol over the Southeast of the US has shown improvement when SCI + SO_2 chemistry is included in the model.[20] The role of SCI + SO_2 chemistry in the atmosphere has also been investigated using observations made on Corsica, in the Mediterranean, where it was found that SCI + SO_2 reactions could be responsible for 10% of the observed H_2SO_4 production during the day and 40% at night.[19] Potential impacts of SCI reactions with SO_2 have also been reported in vehicle exhausts[21] and power plant plumes.[22] However, there have been few measurements of the kinetics of SO_2 oxidation by SCIs other than CH_2OO, and uncertainties in rate coefficients for SCI + SO_2 reactions have been highlighted as a constraint on our understanding of the atmospheric impacts of SCIs and the interpretation of field measurements of H_2SO_4.[16−20,23]

The SCI CH_3CHOO exists in two conformers, *syn*-CH_3CHOO and *anti*-CH_3CHOO, which are separated by a significant barrier to interconversion (~160 kJ mol^{-1})[24] and thus behave as distinct species under ambient conditions.[25,26] The first direct measurements of the reaction kinetics of CH_3CHOO conformers, made using laser flash photolysis of CH_3CHI_2 in the presence of excess O_2 coupled with tunable synchrotron photoionization mass spectrometry (PIMS), demonstrated rapid reactions with SO_2 (R1 and R2).[25]

$$\textit{syn}\text{-}CH_3CHOO + SO_2 \rightarrow \text{products} \quad \text{(R1)}$$

$$\textit{anti}\text{-}CH_3CHOO + SO_2 \rightarrow \text{products} \quad \text{(R2)}$$

The PIMS experiments were performed at 298 K and a total pressure of 4 Torr in He, giving $k_1 = (2.4 \pm 0.3) \times 10^{-11}$ cm^3 s^{-1} and $k_2 = (6.7 \pm 1.0) \times 10^{-11}$ cm^3 s^{-1}. Formation of SO_3 was observed, with a rate that suggested direct production from reactions of CH_3CHOO conformers with SO_2. Subsequent experiments using the PIMS technique at a fixed ionization energy gave a value for k_1 of $(1.7 \pm 0.3) \times 10^{-11}$ cm^3 s^{-1} at 295 K and total pressures between 1 and 2.5 Torr in N_2, with measurements indicating production of acetaldehyde (CH_3CHO) from R1 at a yield of (0.86 ± 0.11) at 2 Torr.[5] The reaction of *syn*-CH_3CHOO with SO_2 has also been investigated by monitoring the kinetics of OH radical production from the decomposition of *syn*-CH_3CHOO occurring in competition with R1, giving $k_1 = (2.5 \pm 0.2) \times 10^{-11}$ cm^3 s^{-1} at 298 K and 10 Torr in Ar.[27]

Experiments using laser flash photolysis of CH_3CHI_2/O_2 mixtures with broadband UV absorption spectroscopy have also indicated that R1 and R2 are rapid.[26,28] A rate coefficient of $(2.0 \pm 0.3) \times 10^{-11}$ cm^3 s^{-1} at 295 K and pressures between 7.5 and 500 Torr of N_2 was reported from experiments in which the conformer-specific contributions to the total absorbance were not resolved.[28] However, the result is expected to be dominated by *syn*-CH_3CHOO on the basis of results from the earlier PIMS experiments,[25] which indicated that *syn*-CH_3CHOO represents 90% of the total CH_3CHOO produced using the photolytic method. Conformer-specific measurements using broadband UV absorption spectroscopy have been achieved in experiments performed at 293 K and a total pressure of 10 Torr in He, giving $k_1 = (2.9 \pm 0.3) \times 10^{-11}$ cm^3 s^{-1} and $k_2 = (2.2 \pm 0.2) \times 10^{-10}$ cm^3 s^{-1}.[26] The conformer-specific UV experiments indicated that *syn*-CH_3CHOO is the dominant conformer produced,[26] in agreement with the earlier PIMS experiments,[25] although a lower yield of 70% was reported, which may result from the different experimental conditions or uncertainties in the UV absorption cross-sections, particularly for *anti*-CH_3CHOO.[26]

There are discrepancies in the literature for values of k_1 and k_2, but studies so far have all taken place at room temperature over a relatively narrow range of pressures (Table 1). Significant conformer dependence is shown for the reactivity of CH_3CHOO with SO_2,[25,26] with studies also showing distinct conformer-dependent reactivity for reactions of asymmetric CIs with H_2O[25,26,29] and acids,[30] as well as differences in their decomposition rates.[31] CH_3CHOO is the simplest Criegee intermediate that exists as two conformers and can therefore be used as a prototype to characterize the reactions of the larger CIs, which requires rate coefficients to be well established across a range of conditions. In this work, we report the kinetics of R1 and R2 at temperatures between 242 and 353 K and pressures between 10 and 600 Torr determined using time-resolved broadband UV absorption spectroscopy.

EXPERIMENTAL SECTION

The kinetics of R1 and R2 were studied as a function of temperature and pressure using laser flash photolysis of $CH_3CHI_2/O_2/N_2/SO_2$ mixtures coupled with time-resolved broadband UV absorption spectroscopy. The experimental apparatus has been described in detail in previous work,[6,31] and only a brief description is given here.

A dilute mixture of a known concentration of SO_2 (Sigma-Aldrich, 99.9%) was prepared manometrically in N_2 (BOC, 99.998%) and stored in a glass bulb before mixing in a gas manifold with N_2 (BOC, 99.998%) and O_2 (BOC, 99.5%) at known flow rates controlled by calibrated mass flow controllers (MKS Instruments). A known fraction of the total gas flow,

https://doi.org/10.1021/acs.jpca.4c00199
J. Phys. Chem. A 2024, 128, 2815−2824

controlled by a needle valve, was then passed through a bubbler containing liquid CH_3CHI_2 (SynHet, 90%) held at a constant temperature in a water bath before being recombined with the rest of the gas flow and passed into a jacketed Pyrex reaction cell. Experiments were performed under pseudo-first-order conditions, with the concentrations of SO_2 in large excess over initial CH_3CHOO concentrations. Concentrations were varied in the range $[CH_3CHI_2] = (2.8–6.0) \times 10^{13}$ cm^{-3}, $[O_2] = (0.6–20) \times 10^{17}$ cm^{-3}, and $[SO_2] = (0.4–5.0) \times 10^{13}$ cm^{-3}, with typical initial $[CH_3CHOO]$ on the order of 10^{12} cm^{-3}.

The reaction cell was 100 cm in length and 3 cm in diameter and sealed with fused silica windows at each end. The temperature of the cell was controlled by flowing liquid from a recirculating thermostatting unit (Huber Unistat 360) through the jacket surrounding the cell and calibrated by measuring the temperature of a flow of N_2, under conditions identical to those used in kinetics experiments, at 5 cm increments along the length of the cell using a K-type thermocouple.[6,31] Pressure in the cell was controlled by a rotary pump (EM2, Edwards) by throttling the exit to the reaction cell and measured by a capacitance manometer (MKS Instruments). The total flow rate through the cell was set to an equivalent of 1200 standard cm^3 min^{-1} (sccm) at 50 Torr and adjusted with pressure to maintain a constant residence time in the cell of ∼2.6 s.

An excimer laser (KrF, Lambda-Physik CompEx 210) with output at λ = 248 nm and typical fluence of 30–40 mJ cm^{-2} was aligned along the length of the reaction cell using a dichroic turning mirror (Edmund Optics) and used to initiate production of *syn*- and *anti*-CH_3CHOO in the cell via reactions R3 and R4a.

$$CH_3CHI_2 + h\nu \rightarrow CH_3CHI + I \quad \text{(R3)}$$

$$CH_3CHI + O_2 \rightarrow \textit{syn}\text{-}CH_3CHOO + I \quad \text{R4a} \quad \text{(R4a)}$$

$$\rightarrow \textit{anti}\text{-}CH_3CHOO + I \quad \text{R4b} \quad \text{(R4b)}$$

A delay generator (SRS DG535) was used to control the timing of the laser, which was operated with a pulse repetition frequency of 0.33 Hz to ensure that the gas mixture in the cell was replaced between each laser pulse.

Absorbing species in the cell were monitored by UV/visible radiation provided by a laser-driven light source (LDLS, Energetiq EQ-99X), which provided ∼10 mW cm^{-2} of light with a near constant radiance from 200 to 800 nm. The LDLS output was collimated by an off-axis parabolic mirror (ThorLabs) and aligned through the reaction cell in a multipass arrangement consisting of ten mirrors (Knight Optical), each of 12 mm diameter, resulting in an effective path length of (595 ± 53) cm for the experiments described in this work, which was determined using the method in our earlier work.[6] Light exiting the cell was passed through a sharp cut-on filter (248 nm RazorEdge ultrasteep long-pass edge filter) to reduce the impact of scattered 248 nm light and focused into a fiber optic via a fiber launcher (Elliot Scientific). Light exiting the fiber optic was directed through a 25 μm slit onto a diffraction grating with 600 grooves/mm and imaged onto a thermoelectrically cooled charge-coupled device (CCD) detector (FER-SCI-1024BRX, Princeton Instruments). Photocharge generated on the CCD was shifted from an illuminated region to a storage region shielded from incoming radiation at set time intervals throughout the reaction, with the experimental setup used in this work giving a spectral resolution of ∼1 nm and a temporal resolution between 70 and 100 μs. Intensity data were typically recorded for 500 photolysis shots and transferred to a PC for analysis.

RESULTS

Absorbance spectra were determined from measured intensity data and related to the concentration of each species present using the Beer–Lambert law (eq 1)

$$A_{\lambda,t} = \ln\left(\frac{I_{\lambda,0}}{I_{\lambda,t}}\right) = \sum_i \sigma_{i,\lambda} c_{i,t} l \quad (1)$$

where $A_{\lambda,t}$ is the total absorbance at wavelength λ and time t, $I_{\lambda,0}$ is the average pre-photolysis light intensity at wavelength λ, $I_{\lambda,t}$ is the post-photolysis light intensity at wavelength λ and time t, $\sigma_{i,\lambda}$ is absorption cross-section of species i at wavelength λ, $c_{i,t}$ is the concentration of species i at time t, and l is the effective path length, which has a value of (595 ± 53) cm for experiments reported in this work.

Figure 1 shows the typical absorbance measured following photolysis, which contains contributions from CH_3CHI_2, *syn*- and *anti*-CH_3CHOO, and IO radicals produced by secondary chemistry within the system. Reference spectra for CH_3CHI_2,[32] *syn*- and *anti*-CH_3CHOO,[26] and IO[33] were fit to the observed absorbance at each time point to determine the concentration of each species throughout the reaction. While absolute concentrations are reported here, it should be noted that uncertainties in the effective path length and absorption cross-sections do not contribute to uncertainties in measured kinetics for the pseudo-first-order conditions employed in this work.

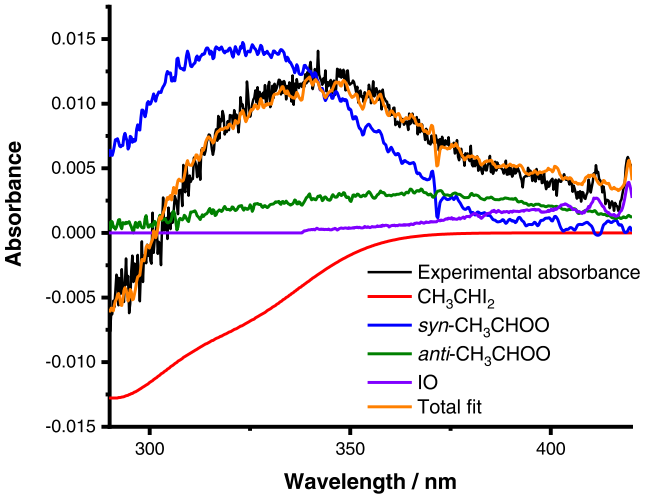

Figure 1. Observed absorbance (black), total fit (orange), and individual contributions from *syn*-CH_3CHOO[26] (blue), *anti*-CH_3CHOO[26] (green), CH_3CHI_2[32] (red), and IO[33] (purple) determined by fitting reference spectra to the observed absorbance using eq 1. For these data, T = 353 K, p = 10 Torr, t = 1 ms, $[CH_3CHI_2] = 6.0 \times 10^{13}$ cm^{-3}. The fit to the observed absorbance for these data gave $\Delta[CH_3CHI_2] = (5.6 \pm 0.07) \times 10^{12}$ cm^{-3}, [*syn*-CH_3CHOO] = (2.3 ± 0.11) × 10^{12} cm^{-3}, [*anti*-CH_3CHOO] = (7.6 ± 0.27) × 10^{11} cm^{-3}, and [IO] = (5.5 ± 0.14) × 10^{11} cm^{-3}.

Figure 2 shows the concentration–time profiles for *syn*- and *anti*-CH_3CHOO in the presence of SO_2, which were each fit according to a first-order kinetic loss (eq 2) convoluted with a Gaussian instrument response function (IRF) to describe the

https://doi.org/10.1021/acs.jpca.4c00199
J. Phys. Chem. A 2024, 128, 2815–2824

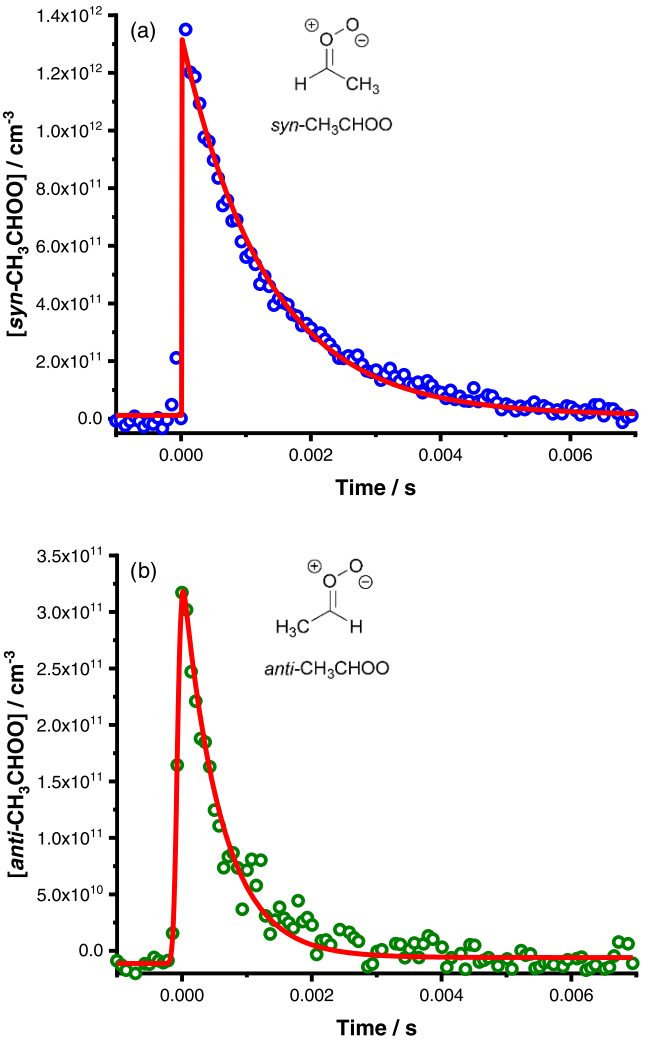

Figure 2. Observed concentration−time profiles for (a) *syn*-CH_3CHOO and (b) *anti*-CH_3CHOO. For these data, T = 298 K, p = 50 Torr, $[SO_2]$ = 1.1 × 10^{13} cm^{-3}, and $[CH_3CHI_2]$ = 2.8 × 10^{13} cm^{-3}. The fits to eq 2 (coupled with the instrument response function as detailed in the Supporting Information) (solid lines) gave an initial concentration of (1.31 ± 0.03) × 10^{12} cm^{-3} and k' = (765 ± 15) s^{-1} for *syn*-CH_3CHOO and an initial concentration of (3.39 ± 0.02) × 10^{11} cm^{-3} and k' = (2280 ± 218) s^{-1} for *anti*-CH_3CHOO. Instrument response parameters were w = (2.99 ± 0.10) × 10^{-5} s and t_c = −(4.80 ± 0.09) × 10^{-5} s for both conformers. Uncertainties are 1σ.

shifting of photocharge on the CCD detector (see the Supporting Information for further details).

$$C_t = C_0 \exp(-k't) \quad (2)$$

where C_t is the concentration of *syn*- or *anti*-CH_3CHOO at time t, C_0 is the initial concentration of the Criegee intermediate conformer, and k' is the rate coefficient describing the sum of first-order losses of the CH_3CHOO conformer and is given by $k' = k_x + k_1[SO_2]$ for *syn*-CH_3CHOO and $k' = k_x + k_2[SO_2]$ for *anti*-CH_3CHOO, where k_x represents losses of *syn*- or *anti*-CH_3CHOO via any reaction or process other than the reaction with SO_2. Unimolecular decomposition and bimolecular reactions with the CH_3CHI_2 precursor contribute significantly to k_x for both *syn*- and *anti*-CH_3CHOO,[31] with potential additional contributions from reactions with iodine atoms, IO, or Criegee−Criegee chemistry as well as diffusion out of the probe region.

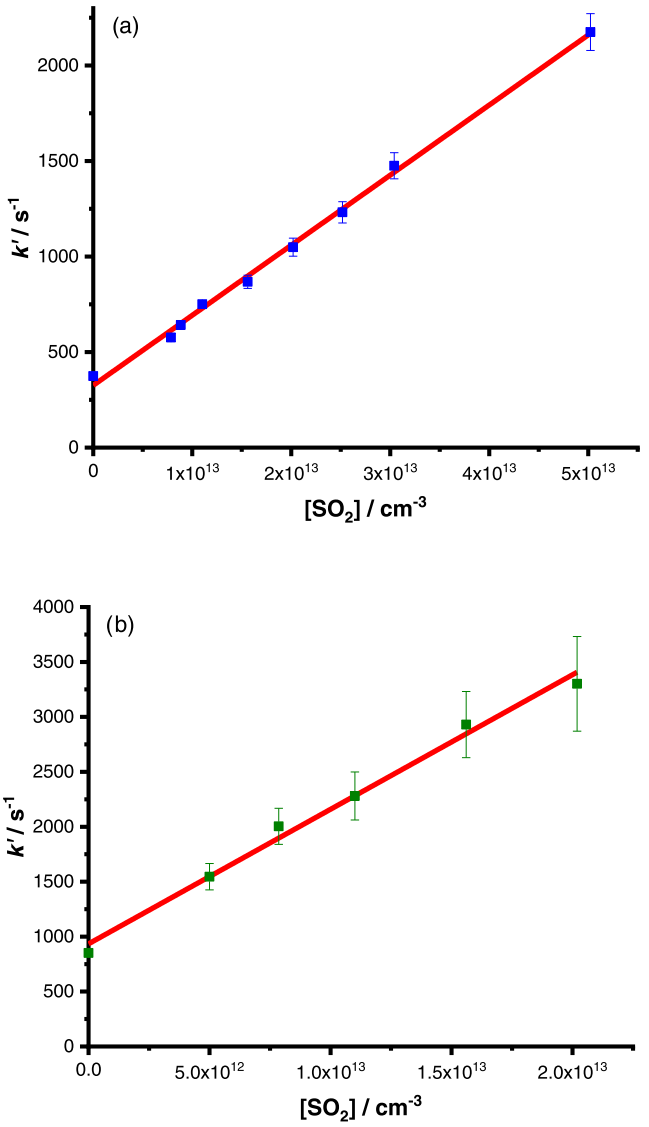

Figure 3. Dependence of k' on $[SO_2]$ at T = 298 K and p = 50 Torr for (a) *syn*-CH_3CHOO and (b) *anti*-CH_3CHOO. Fits to the data (solid lines) gave k_1 = (3.67 ± 0.07) × 10^{-11} cm^3 s^{-1}, with an intercept k_x of (326 ± 18) s^{-1}, and k_2 = (1.22 ± 0.10) × 10^{-10} cm^3 s^{-1}, with an intercept k_x of (934 ± 70) s^{-1}. Uncertainties are 1σ.

Rate coefficients k_1 and k_2 were determined from the dependence of k_1' and k_2' on $[SO_2]$, respectively, with the typical results shown in Figure 3. Potential impacts of second-order losses for the CH_3CHOO conformer through reactions such as CH_3CHOO + CH_3CHOO or CH_3CHOO + I were also investigated by fitting concentration−time profiles to mixed first- and second-order kinetic losses convoluted with the IRF. Results for k_1 and k_2 obtained from the mixed-order fits were within 5% of those obtained from the first-order fits. Further details are given in the Supporting Information. All results reported here were obtained from first-order fits (eq 2).

Figure 4 shows the results for k_1, which are summarized in Table 2. At 298 K, the results demonstrate an increase in k_1 from (3.02 ± 0.32) × 10^{-11} cm^3 s^{-1} at 10 Torr to (4.66 ± 0.52) × 10^{-11} cm^3 s^{-1} at 600 Torr, where the uncertainties represent a combination of the statistical error and the systematic errors resulting from uncertainties in gas flow rates and in the concentration of SO_2, with results at other

https://doi.org/10.1021/acs.jpca.4c00199
J. Phys. Chem. A 2024, 128, 2815−2824

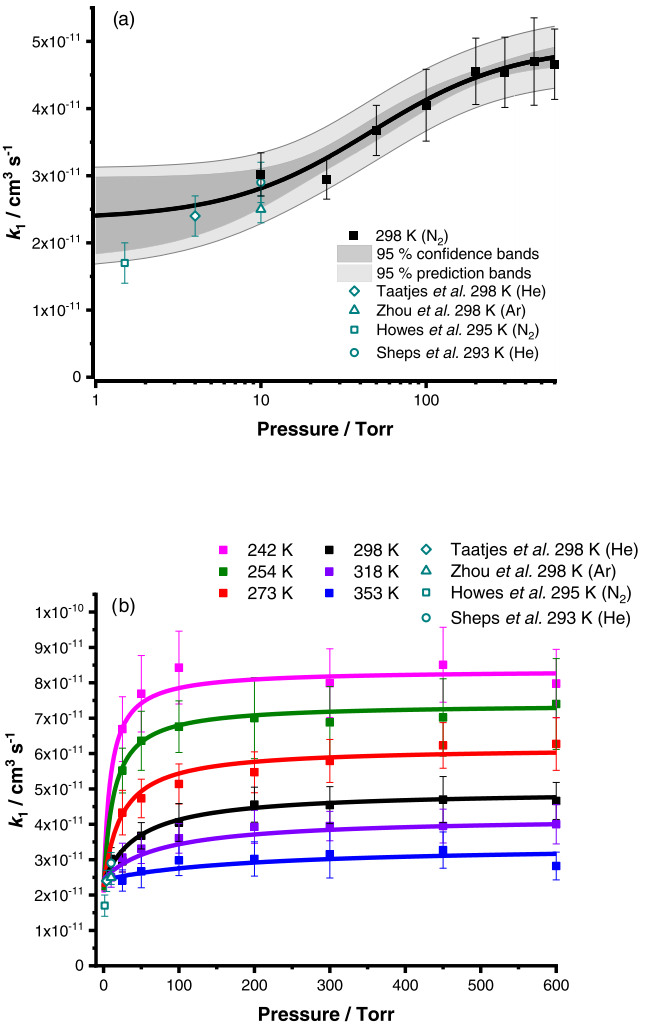

Figure 4. Effects of pressure on k_1 at (a) 298 K and (b) all temperatures studied in this work. Solid lines show the fits to k_1 using eqs 3−6 (which were performed globally using all data for k_1 measured in this work). Previous results reported for k_1 are also shown.[5,25−27] Error bars represent a combination of the statistical error and the systematic errors resulting from uncertainties in gas flow rates and in the concentration of SO_2.

temperatures also showing significant pressure dependence and overall negative temperature dependence. Equations 3−6, which describe a chemical activation mechanism with a non-zero rate coefficient at zero pressure,[34] were fit globally to results obtained in this work for k_1 over all temperatures and pressures to provide a parametrization for use in atmospheric models.

$$k_1 = k_{int} + \frac{(k_\infty - k_{int})k_0[M]}{(k_0[M]) + k_\infty} \quad (3)$$

where k_{int} represents the rate coefficient at zero pressure, k_0 is the low-pressure limiting rate coefficient, and k_∞ is the high-pressure limiting rate coefficient, and these are given by eqs 4−6

$$k_{int} = A_{int} \times \left(\frac{T}{298}\right)^{n_{int}} \quad (4)$$

$$k_0 = A_0 \times \left(\frac{T}{298}\right)^{n_0} \quad (5)$$

$$k_\infty = A_\infty \times \left(\frac{T}{298}\right)^{n_\infty} \quad (6)$$

Fit results gave $A_{int} = (2.35 \pm 0.39) \times 10^{-11}$ cm^3 s^{-1}, $n_{int} = (0.61 \pm 0.79)$, $A_0 = (3.29 \pm 1.30) \times 10^{-29}$ cm^3 s^{-1}, $n_0 = -(9.52 \pm 1.78)$, $A_\infty = (4.95 \pm 0.51) \times 10^{-11}$ cm^3 s^{-1}, and $n_\infty = -(2.52 \pm 0.29)$.

The fits of eqs 3−6 indicate a value for k_1 of $(4.80 \pm 0.46) \times 10^{-11}$ cm^3 s^{-1} at 298 K and 760 Torr. The pressure dependence observed in this work reconciles discrepancies between values for k_1 reported at room temperature in previous work[5,25−27] at pressures below 10 Torr, as shown in Figure 4. While kinetics reported by Smith et al.[28] at 295 K over the pressure range of 7.5−500 Torr are in broad agreement with low pressure values for k_1 reported in this work and in previous work, Smith et al. were unable to distinguish between the *syn*- and *anti*-conformers, so the rate coefficient reported will contain contributions from the reactivity of both *syn*-CH_3CHOO and *anti*-CH_3CHOO.

Figure 5 and Table 2 summarize the results obtained in this work for k_2. In contrast to the results for k_1, no significant dependence of k_2 on the temperature or pressure was observed. At 298 K, results gave a mean value for k_2 of $(1.15 \pm 0.16) \times 10^{-10}$ cm^3 s^{-1} between 10 and 600 Torr, with results over all temperatures and pressures giving a mean value of $(1.18 \pm 0.21) \times 10^{-10}$ cm^3 s^{-1}. The effect of pressure on k_2 at each temperature is shown in Figure S3 in the Supporting Information.

The kinetics of R2 have been reported in two previous studies[25,26] at room temperature. Taatjes et al.[25] performed experiments at 4 Torr using the PIMS technique and reported a value for k_2 of $(6.7 \pm 1.0) \times 10^{-11}$ cm^3 s^{-1}, while Sheps et al.[26] performed experiments at 10 Torr using cavity-enhanced UV absorption spectroscopy and reported a value for k_2 of $(2.2 \pm 0.2) \times 10^{-10}$ cm^3 s^{-1}. Differences between the studies reflect the challenges associated with measuring such rapid kinetics, with the lack of dependence of k_2 on temperature and pressure observed in this work potentially indicating that the kinetics for R2 are controlled by collision-limited or capture-limited kinetics. The difference in behavior between the *syn*- and *anti*-conformers is potentially influenced by lower steric hindrance for the *anti*-conformer, coupled with the higher ground state energy for *anti*-CH_3CHOO by ∼15 kJ mol^{-1}[24] compared to *syn*-CH_3CHOO and a higher dipole moment for *anti*-CH_3CHOO than *syn*-CH_3CHOO (5.53 D compared to 4.69 D, calculated at the B3LYP/AVTZ level of theory[35]).

Figure 6 compares the experimental results for k_2 with estimated values using a collision model (eq 7) and a capture model (eq 8).

$$k_{col} = \pi(r_{CI} + r_{SO_2})^2 \sqrt{\frac{8k_BT}{\pi\mu}} \quad (7)$$

where r_{CI} and r_{SO_2} are the effective radii of *anti*-CH_3CHOO[36] and SO_2,[37] respectively, k_B is the Boltzmann constant, T is the temperature, and μ is the reduced mass. The effective radius for *anti*-CH_3CHOO was assumed to be the same as that reported in the literature for *syn*-CH_3CHOO.[36]

https://doi.org/10.1021/acs.jpca.4c00199
J. Phys. Chem. A 2024, 128, 2815−2824

Table 2. Summary of Results for k_1 and k_2[a]

T/K	p/Torr	$[CH_3CHI_2]/10^{13}$ cm^{-3}	$[SO_2]/10^{13}$ cm^{-3}	$k_1/10^{-11}$ cm^3 s^{-1}	$k_2/10^{-10}$ cm^3 s^{-1}
242	25	3.0−4.1	0.6−3.1	6.69 ± 0.92	1.13 ± 0.13
	50			7.69 ± 1.08	1.17 ± 0.22
	100			8.43 ± 1.03	1.06 ± 0.17
	300			7.99 ± 0.97	1.06 ± 0.19
	450			8.51 ± 1.06	1.16 ± 0.25
	600			7.98 ± 0.97	
254	25	5.2−5.9	0.9−3.2	5.52 ± 0.63	0.90 ± 0.14
	50			6.36 ± 0.83	1.01 ± 0.20
	100			6.76 ± 0.73	1.00 ± 0.10
	200			7.00 ± 1.14	1.00 ± 0.18
	300			6.88 ± 1.02	
	450			7.02 ± 1.09	
	600			7.4 ± 1.28	
273	25	3.4−4.3	0.6−2.7	4.33 ± 0.63	1.29 ± 0.14
	50			4.73 ± 0.55	1.50 ± 0.28
	100			5.14 ± 0.57	1.54 ± 0.17
	200			5.47 ± 0.58	1.56 ± 0.18
	300			5.79 ± 0.61	
	450			6.23 ± 0.64	1.32 ± 0.21
	600			6.27 ± 0.74	
298	10	2.8−3.7	0.5−5.0	3.02 ± 0.32	1.04 ± 0.13
	25			3.00 ± 0.30	1.33 ± 0.17
	50			3.67 ± 0.37	1.22 ± 0.16
	100			4.05 ± 0.54	1.19 ± 0.17
	200			4.55 ± 0.49	1.08 ± 0.14
	300			4.54 ± 0.52	1.10 ± 0.20
	450			4.70 ± 0.65	1.26 ± 0.16
	600			4.66 ± 0.52	0.96 ± 0.16
318	10	4.1−5.3	0.7−4.1	2.50 ± 0.48	1.22 ± 0.22
	25			3.06 ± 0.41	1.42 ± 0.15
	50			3.31 ± 0.42	1.20 ± 0.21
	100			3.60 ± 0.42	1.05 ± 0.17
	200			3.93 ± 0.47	1.32 ± 0.22
	300			3.95 ± 0.42	1.41 ± 0.17
	450			3.95 ± 0.48	1.11 ± 0.20
	600			4.00 ± 0.56	1.08 ± 0.26
353	10	5.1−6.0	0.4−2.4		1.29 ± 0.20
	25			2.41 ± 0.30	1.09 ± 0.17
	50			2.67 ± 0.47	1.22 ± 0.25
	100			2.98 ± 0.43	1.10 ± 0.28
	200			3.02 ± 0.48	1.17 ± 0.19
	300			3.15 ± 0.67	1.13 ± 0.13
	450			3.27 ± 0.51	1.40 ± 0.25
	600			2.82 ± 0.39	0.88 ± 0.12

[a]Uncertainties represent a combination of the 1σ statistical error and the systematic errors resulting from uncertainties in gas flow rates and in the concentration of SO_2.

$$k_{capt} = C\sqrt{\frac{\pi}{\mu}}(D_{CI}D_{SO_2})^{2/3}(k_BT)^{-1/6} \quad (8)$$

where C is a constant (4.08 for the case of isotropic capture)[35,38] and D_{CI} and D_{SO_2} are the dipole moments of *anti*-CH_3CHOO[35] and SO_2,[39] respectively.

The experimental results for k_2 obtained in this work are lower than the estimated rate coefficients using either the collision model or the capture model, with experimental values a factor of ∼2 lower than those calculated from collision theory and a factor of ∼6 lower than those calculated from capture theory. However, the calculated values do offer some insight into the kinetics and suggest that R2 is close to the collision limit.

The reaction between *syn*-CH_3CHOO and SO_2 has been investigated using theoretical approaches, which indicate a barrierless reaction with a 98% yield of acetaldehyde (CH_3CHO) + SO_3 at 298 K and 200 Torr of He and a rate coefficient for CH_3CHO + SO_3 production of 4.49×10^{-11} cm^3 s^{-1} at 298 K.[13] However, the possible impacts of pressure were not fully discussed, and the reaction of *anti*-CH_3CHOO + SO_2 was not considered. The calculations[13] predicted a positive temperature dependence for reactions of CH_2OO, *syn*-CH_3CHOO, and $(CH_3)_2COO$ with SO_2, despite the reactions being barrierless, and this is in contrast to the

https://doi.org/10.1021/acs.jpca.4c00199
J. Phys. Chem. A 2024, 128, 2815−2824

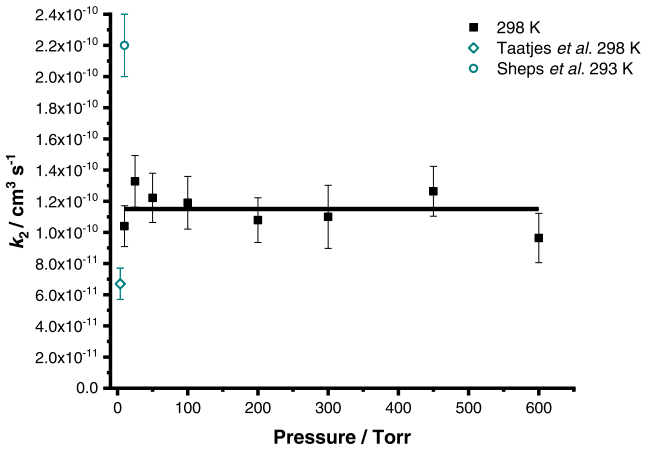

Figure 5. Effects of pressure on k_2 at 298 K. The solid line shows the mean value for k_2 at 298 K ($(1.15 \pm 0.16) \times 10^{-10}$ cm^3 s^{-1}). Previous results reported for k_2 are also shown. Error bars represent a combination of the statistical error and the systematic errors resulting from uncertainties in gas flow rates and in the concentration of SO_2.

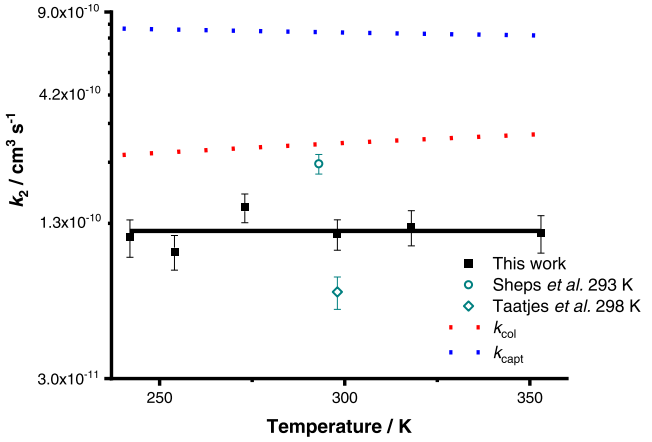

Figure 6. Mean values for k_2 determined at each temperature. The solid line represents that the mean value for k_2 over all conditions investigated in this work is $(1.18 \pm 0.21) \times 10^{-10}$ cm^3 s^{-1}. Previous results reported for k_2 and rate coefficients calculated using collision theory (k_{col}, red dashed line) and capture theory (k_{capt}, blue dashed line) are also shown. Error bars represent a combination of the statistical error and the systematic errors resulting from uncertainties in gas flow rates and in the concentration of SO_2.

experimental results for *syn*-CH_3CHOO + SO_2 obtained in this work, our previous experiments for CH_2OO + SO_2,[6] and experimental results for $(CH_3)_2COO$ + SO_2[40] (see the Supporting Information for further details). Where potential impacts of pressure have been considered in detail in theoretical studies of SCI + SO_2 reactions, there is an agreement with the lack of observed pressure dependence in the kinetics for CH_2OO + SO_2 under atmospheric conditions,[3,4,11,12] but there are differences in the predicted pressure dependence of the reaction between $(CH_3)_2COO$ and SO_2.[11,12] Vereecken et al. suggested that >80% of the SOZ formed by $(CH_3)_2COO$ + SO_2 undergoes prompt decomposition to acetone ($CH_3C(O)CH_3$) and SO_3 at 298 K and a pressure of 4 Torr, while >97% of the SOZ collisionally stabilizes at 298 K and 760 Torr, with the difference compared to CH_2OO + SO_2 attributed to the greater number of degrees of freedom in the SOZ formed via $(CH_3)_2COO$ + SO_2, which would also be relevant to the comparison between the SOZ formed via CH_2OO + SO_2 and those from reactions of CH_3CHOO conformers with SO_2. However, Kuwata et al. calculated a different potential energy surface for the reaction between $(CH_3)_2COO$ and SO_2 compared to that reported by Vereecken et al., and thus a different mechanism for the reaction, with calculations predicting no significant collisional stabilization of the SOZ at 298 K and pressures below 10^4 Torr and SO_3 yields greater than 96% at 298 K and pressures from 1 to 760 Torr. Experimental measurements of the kinetics for $(CH_3)_2COO$ + SO_2 have indicated significant pressure dependence and negative temperature dependence under atmospheric conditions,[40−42] similar to the observations in this work for the reaction between *syn*-CH_3CHOO and SO_2. Differences between theoretical approaches and between experiments and theory indicate that the application of theory to the prediction of SCI kinetics remains a challenge.

■ ATMOSPHERIC IMPLICATIONS

The atmospheric impacts of CH_3CHOO conformer reactions with SO_2 depend on the competition with other CH_3CHOO conformer reactions, which are expected to be dominated by unimolecular decomposition for *syn*-CH_3CHOO and reaction with water vapor for *anti*-CH_3CHOO.[31,43−45] Figure 7 compares the pseudo-first-order losses for CH_3CHOO conformers through unimolecular decomposition and reactions with SO_2 and water vapor for a range of SO_2 and water vapor concentrations as a function of temperature at 760 Torr. Rate coefficients for unimolecular decomposition (k_{dec}) were taken from our recent work,[31] and those for reactions with SO_2 (k_{SO_2}) were taken from those determined in this work. Rate coefficients for reactions with water vapor (k_{H2O} and $k_{(H_2O)_2}$) were based on the upper limit for *syn*-CH_3CHOO + H_2O reported by Sheps et al. at 298 K,[26] which forms the basis of the current IUPAC recommendation,[3] and temperature-dependent measurements for *anti*-CH_3CHOO + H_2O and *anti*-CH_3CHOO + $(H_2O)_2$ reported by Lin et al.[45] Water dimer concentrations were calculated from the monomer concentration using equilibrium constants reported by Ruscic et al.[46] There are no current reports of rate coefficients or upper limits for a possible reaction of *syn*-CH_3CHOO with water dimers, and it should be noted that current IUPAC recommendations[3] for *anti*-CH_3CHOO reactions with water vapor do not extend beyond 298 K, owing to uncertainties in temperature-dependent measurements, which will impact the analysis shown in Figure 7. For *anti*-CH_3CHOO, results show that the reaction with water vapor will dominate under all conditions relevant to the troposphere, but chamber studies employing high SO_2 concentrations and low humidity will need to consider the impact of R2. For *syn*-CH_3CHOO, the reaction with SO_2 will be competitive with other losses in the atmosphere in areas with high SO_2 concentrations and low humidity, particularly at low temperatures, contributing to the atmospheric oxidation of SO_2. The pressure dependence of k_1 indicates that there may be significant collisional stabilization of the SOZ produced in the reaction between *syn*-CH_3CHOO and SO_2, potentially limiting the production of SO_3 and subsequently H_2SO_4. However, the fate of the SOZ is uncertain, and even if there is significant stabilization of the SOZ, it may still contribute to the atmospheric production of H_2SO_4 through subsequent chemistry. A more detailed assessment of the atmospheric impacts of CI reactions with

https://doi.org/10.1021/acs.jpca.4c00199
J. Phys. Chem. A 2024, 128, 2815−2824

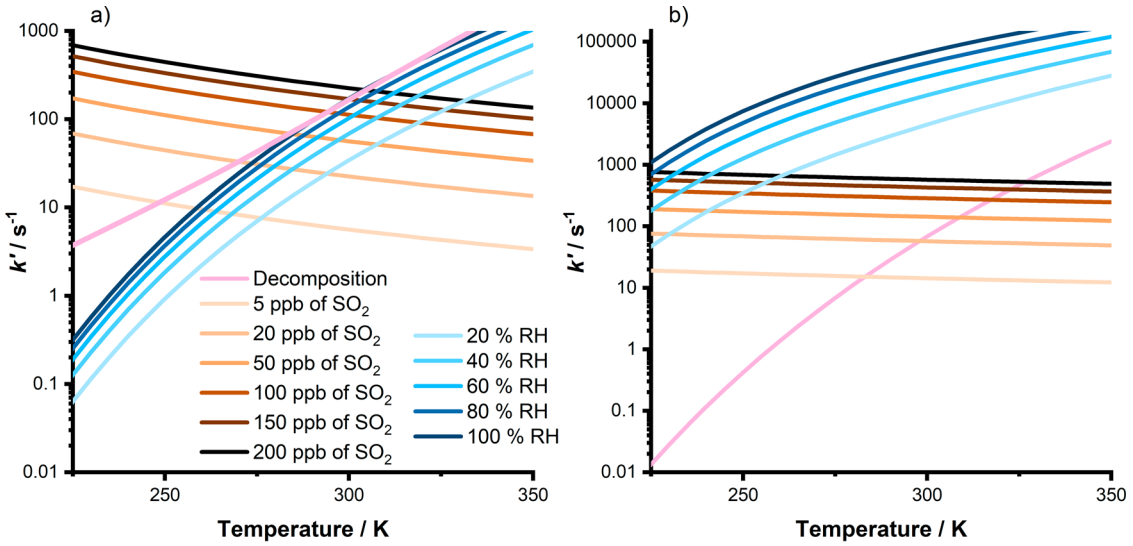

Figure 7. Pseudo-first-order losses of (a) *syn*-CH_3CHOO and (b) *anti*-CH_3CHOO through reaction with SO_2 (orange), reaction with water vapor (blue), and unimolecular decomposition (pink) at a total pressure of 760 Torr. Pseudo-first-order losses were calculated as described in the main text.

SO_2 would benefit from further experimental investigation of the nature and yields of the products, particularly as a function of pressure.

CONCLUSIONS

The kinetics of *syn*- and *anti*-CH_3CHOO reactions with SO_2 have been investigated in the temperature range from 242 to 353 K at pressures between 10 and 600 Torr using laser flash photolysis of $CH_3CHI_2/O_2/N_2/SO_2$ gas mixtures coupled with time-resolved broadband UV absorption spectroscopy.

Results for *syn*-CH_3CHOO + SO_2 show that the kinetics are pressure-dependent, with a negative dependence on temperature. The kinetics can be parametrized by a model that indicates a role for chemical activation, which gives a rate coefficient of $k_1 = (4.80 \pm 0.46) \times 10^{-11}$ cm^3 s^{-1} at 298 K and 760 Torr. The observed pressure dependence reconciles apparent discrepancies in previous measurements of *syn*-CH_3CHOO + SO_2 kinetics performed at ∼298 K but at different pressures.

Kinetics of the reaction between *anti*-CH_3CHOO and SO_2 display no significant dependence on temperature or pressure over the ranges investigated. Results give a mean value for k_2 of $(1.15 \pm 0.16) \times 10^{-10}$ cm^3 s^{-1} at 298 K and $(1.18 \pm 0.21) \times 10^{-10}$ cm^3 s^{-1} over all conditions studied in this work.

Comparisons with unimolecular decomposition kinetics of *syn*- and *anti*-CH_3CHOO and reactions with water vapor under typical atmospheric conditions indicate that the reaction with SO_2 will play an enhanced role in the removal of the *syn*-CH_3CHOO in areas of low humidity and at low temperatures and the removal of *anti*-CH_3CHOO is dominated by its reaction with water vapor under all conditions relevant to the troposphere.

ASSOCIATED CONTENT

Supporting Information

The Supporting Information is available free of charge at https://pubs.acs.org/doi/10.1021/acs.jpca.4c00199.

Description of the instrument response function, comparison of first- and mixed-order analysis, effects of pressure on k_2 across the studied temperature range, comparison to theoretical calculations, and summary of experimental data (PDF)

AUTHOR INFORMATION

Corresponding Author

Daniel Stone − *School of Chemistry, University of Leeds, Leeds LS2 9JT, U.K.;* orcid.org/0000-0001-5610-0463; Email: d.stone@leeds.ac.uk

Authors

Rachel E. Lade − *School of Chemistry, University of Leeds, Leeds LS2 9JT, U.K.;* orcid.org/0000-0003-1773-5655

Lavinia Onel − *School of Chemistry, University of Leeds, Leeds LS2 9JT, U.K.;* orcid.org/0000-0002-0637-9141

Mark A. Blitz − *School of Chemistry, University of Leeds, Leeds LS2 9JT, U.K.; National Centre for Atmospheric Science, University of Leeds, Leeds LS2 9JT, U.K.;* orcid.org/0000-0001-6710-4021

Paul W. Seakins − *School of Chemistry, University of Leeds, Leeds LS2 9JT, U.K.;* orcid.org/0000-0002-4335-8593

Complete contact information is available at: https://pubs.acs.org/10.1021/acs.jpca.4c00199

Notes

The authors declare no competing financial interest.

ACKNOWLEDGMENTS

The authors thank the Natural Environment Research Council (NERC) for funding (grant references NE/L010798/1 and NE/P012876/1).

REFERENCES

(1) Johnson, D.; Marston, G. The gas-phase ozonolysis of unsaturated volatile organic compounds in the troposphere. *Chem. Soc. Rev.* **2008**, *37* (4), 699−716.

(2) Vereecken, L. Lifting the Veil on an Old Mystery. *Science* **2013**, *340* (6129), 154−155.

(3) Cox, R. A.; Ammann, M.; Crowley, J. N.; Herrmann, H.; Jenkin, M. E.; McNeill, V. F.; Mellouki, A.; Troe, J.; Wallington, T. J.

Evaluated kinetic and photochemical data for atmospheric chemistry: Volume VII − Criegee intermediates. *Atmos. Chem. Phys.* **2020**, *20* (21), 13497−13519.
(4) Stone, D.; Blitz, M.; Daubney, L.; Howes, N. U. M.; Seakins, P. Kinetics of CH_2OO reactions with SO_2, NO_2, NO, H_2O and CH_3CHO as a function of pressure. *Phys. Chem. Chem. Phys.* **2014**, *16* (3), 1139−1149.
(5) Howes, N. U. M.; Mir, Z. S.; Blitz, M. A.; Hardman, S.; Lewis, T. R.; Stone, D.; Seakins, P. W. Kinetic studies of C1 and C2 Criegee intermediates with SO_2 using laser flash photolysis coupled with photoionization mass spectrometry and time resolved UV absorption spectroscopy. *Phys. Chem. Chem. Phys.* **2018**, *20* (34), 22218−22227.
(6) Onel, L.; Lade, R.; Mortiboy, J.; Blitz, M. A.; Seakins, P. W.; Heard, D. E.; Stone, D. Kinetics of the gas phase reaction of the Criegee intermediate CH_2OO with SO_2 as a function of temperature. *Phys. Chem. Chem. Phys.* **2021**, *23* (35), 19415−19423.
(7) Stone, D.; Blitz, M.; Daubney, L.; Ingham, T.; Seakins, P. CH_2OO Criegee biradical yields following photolysis of CH_2I_2 in O_2. *Phys. Chem. Chem. Phys.* **2013**, *15* (44), 19119−19124.
(8) Wang, Y.-Y.; Dash, M. R.; Chung, C.-Y.; Lee, Y.-P. Detection of transient infrared absorption of SO_3 and 1,3,2-dioxathietane-2,2-dioxide [cyc-$(CH_2)O(SO_2)O$] in the reaction CH_2OO+SO_2. *J. Chem. Phys.* **2018**, *148* (6), No. 064301.
(9) Mir, Z. S.; Jamieson, M.; Greenall, N. R.; Seakins, P. W.; Blitz, M. A.; Stone, D. Identification, monitoring, and reaction kinetics of reactive trace species using time-resolved mid-infrared quantum cascade laser absorption spectroscopy: development, characterisation, and initial results for the CH_2OO Criegee intermediate. *Atmos. Meas. Tech.* **2022**, *15* (9), 2875−2887.
(10) Aplincourt, P.; Ruiz-López, M. F. Theoretical Investigation of Reaction Mechanisms for Carboxylic Acid Formation in the Atmosphere. *J. Am. Chem. Soc.* **2000**, *122* (37), 8990−8997.
(11) Vereecken, L.; Harder, H.; Novelli, A. The reaction of Criegee intermediates with NO, RO_2, and SO_2, and their fate in the atmosphere. *Phys. Chem. Chem. Phys.* **2012**, *14* (42), 14682−14695.
(12) Kuwata, K. T.; Guinn, E. J.; Hermes, M. R.; Fernandez, J. A.; Mathison, J. M.; Huang, K. A Computational Re-examination of the Criegee Intermediate−Sulfur Dioxide Reaction. *J. Phys. Chem. A* **2015**, *119* (41), 10316−10335.
(13) Manonmani, G.; Sandhiya, L.; Senthilkumar, K. Reaction of Criegee Intermediates with SO_2—A Possible Route for Sulfurous Acid Formation in the Atmosphere. *ACS Earth Space Chem.* **2023**, *7* (10), 1890−1904.
(14) Kurtén, T.; Lane, J. R.; Jørgensen, S.; Kjaergaard, H. G. A Computational Study of the Oxidation of SO_2 to SO_3 by Gas-Phase Organic Oxidants. *J. Phys. Chem. A* **2011**, *115* (31), 8669−8681.
(15) Jiang, L.; Xu, Y.-s.; Ding, A.-z. Reaction of Stabilized Criegee Intermediates from Ozonolysis of Limonene with Sulfur Dioxide: Ab Initio and DFT Study. *J. Phys. Chem. A* **2010**, *114* (47), 12452−12461.
(16) Mauldin Iii, R. L.; Berndt, T.; Sipilä, M.; Paasonen, P.; Petäjä, T.; Kim, S.; Kurtén, T.; Stratmann, F.; Kerminen, V. M.; Kulmala, M. A new atmospherically relevant oxidant of sulphur dioxide. *Nature* **2012**, *488* (7410), 193−196.
(17) Boy, M.; Mogensen, D.; Smolander, S.; Zhou, L.; Nieminen, T.; Paasonen, P.; Plass-Dülmer, C.; Sipilä, M.; Petäjä, T.; Mauldin, L.; et al. Oxidation of SO_2 by stabilized Criegee intermediate (sCI) radicals as a crucial source for atmospheric sulfuric acid concentrations. *Atmos. Chem. Phys.* **2013**, *13* (7), 3865−3879.
(18) Kim, S.; Guenther, A.; Lefer, B.; Flynn, J.; Griffin, R.; Rutter, A. P.; Gong, L.; Cevik, B. K. Potential Role of Stabilized Criegee Radicals in Sulfuric Acid Production in a High Biogenic VOC Environment. *Environ. Sci. Technol.* **2015**, *49* (6), 3383−3391.
(19) Kukui, A.; Chartier, M.; Wang, J.; Chen, H.; Dusanter, S.; Sauvage, S.; Michoud, V.; Locoge, N.; Gros, V.; Bourrianne, T.; et al. Role of Criegee intermediates in the formation of sulfuric acid at a Mediterranean (Cape Corsica) site under influence of biogenic emissions. *Atmos. Chem. Phys.* **2021**, *21* (17), 13333−13351.
(20) Sarwar, G.; Simon, H.; Fahey, K.; Mathur, R.; Goliff, W. S.; Stockwell, W. R. Impact of sulfur dioxide oxidation by Stabilized Criegee Intermediate on sulfate. *Atmos. Environ.* **2014**, *85*, 204−214.
(21) Liu, T.; Wang, X.; Hu, Q.; Deng, W.; Zhang, Y.; Ding, X.; Fu, X.; Bernard, F.; Zhang, Z.; Lü, S.; et al. Formation of secondary aerosols from gasoline vehicle exhaust when mixing with SO_2. *Atmos. Chem. Phys.* **2016**, *16* (2), 675−689.
(22) Meidan, D.; Holloway, J. S.; Edwards, P. M.; Dubé, W. P.; Middlebrook, A. M.; Liao, J.; Welti, A.; Graus, M.; Warneke, C.; Ryerson, T. B.; et al. Role of Criegee Intermediates in Secondary Sulfate Aerosol Formation in Nocturnal Power Plant Plumes in the Southeast US. *ACS Earth Space Chem.* **2019**, *3* (5), 748−759.
(23) Percival, C. J.; Welz, O.; Eskola, A. J.; Savee, J. D.; Osborn, D. L.; Topping, D. O.; Lowe, D.; Utembe, S. R.; Bacak, A.; M c Figgans, G.; et al. Regional and global impacts of Criegee intermediates on atmospheric sulphuric acid concentrations and first steps of aerosol formation. *Faraday Discuss.* **2013**, *165* (0), 45−73.
(24) Kuwata, K. T.; Hermes, M. R.; Carlson, M. J.; Zogg, C. K. Computational Studies of the Isomerization and Hydration Reactions of Acetaldehyde Oxide and Methyl Vinyl Carbonyl Oxide. *J. Phys. Chem. A* **2010**, *114* (34), 9192−9204.
(25) Taatjes, C. A.; Welz, O.; Eskola, A. J.; Savee, J. D.; Scheer, A. M.; Shallcross, D. E.; Rotavera, B.; Lee, E. P. F.; Dyke, J. M.; Mok, D. K. W.; et al. Direct Measurements of Conformer-Dependent Reactivity of the Criegee Intermediate CH_3CHOO. *Science* **2013**, *340* (6129), 177.
(26) Sheps, L.; Scully, A. M.; Au, K. UV absorption probing of the conformer-dependent reactivity of a Criegee intermediate CH_3CHOO. *Phys. Chem. Chem. Phys.* **2014**, *16* (48), 26701−26706.
(27) Zhou, X.; Liu, Y.; Dong, W.; Yang, X. Unimolecular Reaction Rate Measurement of *syn*-CH_3CHOO. *J. Phys. Chem. Lett.* **2019**, *10* (17), 4817−4821.
(28) Smith, M. C.; Ting, W.-L.; Chang, C.-H.; Takahashi, K.; Boering, K. A.; Lin, J. J.-M. UV absorption spectrum of the C2 Criegee intermediate CH_3CHOO. *J. Chem. Phys.* **2014**, *141* (7), No. 074302.
(29) Anglada, J. M.; González, J.; Torrent-Sucarrat, M. Effects of the substituents on the reactivity of carbonyl oxides. A theoretical study on the reaction of substituted carbonyl oxides with water. *Phys. Chem. Chem. Phys.* **2011**, *13* (28), 13034−13045.
(30) Welz, O.; Eskola, A. J.; Sheps, L.; Rotavera, B.; Savee, J. D.; Scheer, A. M.; Osborn, D. L.; Lowe, D.; Murray Booth, A.; Xiao, P.; et al. Rate Coefficients of C1 and C2 Criegee Intermediate Reactions with Formic and Acetic Acid Near the Collision Limit: Direct Kinetics Measurements and Atmospheric Implications. *Angew. Chem., Int. Ed.* **2014**, *53* (18), 4547−4550.
(31) Robinson, C.; Onel, L.; Newman, J.; Lade, R.; Au, K.; Sheps, L.; Heard, D. E.; Seakins, P. W.; Blitz, M. A.; Stone, D. Unimolecular Kinetics of Stabilized CH_3CHOO Criegee Intermediates: syn-CH_3CHOO Decomposition and anti-CH_3CHOO Isomerization. *J. Phys. Chem. A* **2022**, *126* (39), 6984−6994.
(32) Sander, S. P.; Abbatt, J. P. D.; Barker, J. R.; Burkholder, J. B.; Friedl, R. R.; Golden, D. M.; Huie, R. E.; Kolb, C. E.; Kurylo, M. J.; Moortgat, G. K.; Orkin, V. L.; Wine, P. H. *Chemical Kinetics and Photochemical Data for Use in Atmospheric Studies, Evaluation Number 17*; JPL publication 10-6, 2011.
(33) Harwood, M. H.; Burkholder, J. B.; Hunter, M.; Fox, R. W.; Ravishankara, A. R. Absorption Cross Sections and Self-Reaction Kinetics of the IO Radical. *J. Phys. Chem. A* **1997**, *101* (5), 853−863.
(34) Tyndall, G. S.; Orlando, J. J.; Wallington, T. J.; Hurley, M. D. Pressure dependence of the rate coefficients and product yields for the reaction of CH_3CO radicals with O_2. *Int. J. Chem. Kinet.* **1997**, *29* (9), 655−663.
(35) Chhantyal-Pun, R.; Rotavera, B.; McGillen, M. R.; Khan, M. A. H.; Eskola, A. J.; Caravan, R. L.; Blacker, L.; Tew, D. P.; Osborn, D. L.; Percival, C. J.; et al. Criegee Intermediate Reactions with Carboxylic Acids: A Potential Source of Secondary Organic Aerosol in the Atmosphere. *ACS Earth Space Chem.* **2018**, *2* (8), 833−842.

(36) Takahashi, K. Theoretical analysis on reactions between *syn*-methyl Criegee intermediate and amino alcohols. *J. Chin. Chem. Soc.* **2022**, *69* (1), 184−192.
(37) Linstrom, P. J.; Mallard, W. G., Eds., NIST Chemistry WebBook. *NIST Standard Reference Database Number 69*; National Institute of Standards and Technology: Gaithersburg MD, 20899. http://webbook.nist.gov (accessed Dec, 2023).
(38) Maergoiz, A. I.; Nikitin, E. E.; Troe, J.; Ushakov, V. G. Classical trajectory and adiabatic channel study of the transition from adiabatic to sudden capture dynamics. III. Dipole−dipole capture. *J. Chem. Phys.* **1996**, *105* (15), 6277−6284.
(39) Patel, D.; Margolese, D.; Dykea, T. R. Electric dipole moment of SO_2 in ground and excited vibrational states. *J. Chem. Phys.* **1979**, *70* (6), 2740−2747.
(40) Smith, M. C.; Chao, W.; Takahashi, K.; Boering, K. A.; Lin, J. J.-M. Unimolecular Decomposition Rate of the Criegee Intermediate $(CH_3)_2COO$ Measured Directly with UV Absorption Spectroscopy. *J. Phys. Chem. A* **2016**, *120* (27), 4789−4798.
(41) Chhantyal-Pun, R.; Welz, O.; Savee, J. D.; Eskola, A. J.; Lee, E. P. F.; Blacker, L.; Hill, H. R.; Ashcroft, M.; Khan, M. A. H.; Lloyd-Jones, G. C.; et al. Direct Measurements of Unimolecular and Bimolecular Reaction Kinetics of the Criegee Intermediate $(CH_3)_2COO$. *J. Phys. Chem. A* **2017**, *121* (1), 4−15.
(42) Huang, H.-L.; Chao, W.; Lin, J. J.-M. Kinetics of a Criegee intermediate that would survive high humidity and may oxidize atmospheric SO_2. *Proc. Natl. Acad. Sci. U.S.A.* **2015**, *112* (35), 10857−10862.
(43) Chhantyal-Pun, R.; Khan, M. A. H.; Taatjes, C. A.; Percival, C. J.; Orr-Ewing, A. J.; Shallcross, D. E. Criegee intermediates: production, detection and reactivity. *Int. Rev. Phys. Chem.* **2020**, *39* (3), 385−424.
(44) Vereecken, L.; Novelli, A.; Taraborrelli, D. Unimolecular decay strongly limits the atmospheric impact of Criegee intermediates. *Phys. Chem. Chem. Phys.* **2017**, *19* (47), 31599−31612.
(45) Lin, L.-C.; Chao, W.; Chang, C.-H.; Takahashi, K.; Lin, J. J.-M. Temperature dependence of the reaction of anti-CH_3CHOO with water vapor. *Phys. Chem. Chem. Phys.* **2016**, *18* (40), 28189−28197.
(46) Ruscic, B. Active Thermochemical Tables: Water and Water Dimer. *J. Phys. Chem. A* **2013**, *117* (46), 11940−11953.

https://doi.org/10.1021/acs.jpca.4c00199
J. Phys. Chem. A 2024, 128, 2815−2824